MDPI

Article

Dynamic Line Scan Thermography Optimisation Using Response Surfaces Implemented on PVC Flat Bottom Hole Plates

Simon Verspeek [1,*], Jona Gladines [1], Bart Ribbens [1], Xavier Maldague [2] and Gunther Steenackers [1]

1 Op3Mech Research Group, Faculty of Applied Engineering, University of Antwerp, 2020 Antwerp, Belgium; Jona.Gladines@uantwerpen.be (J.G.); Bart.Ribbens@uantwerpen.be (B.R.); Gunther.Steenackers@uantwerpen.be (G.S.)
2 Department of Electrical and Computer Engineering, Computer Vision and Systems Laboratory, Université Laval, Quebec City, QC G1V 0A6, Canada; xavier.maldague@gel.ulaval.ca
* Correspondence: Simon.Verspeek@uantwerpen.be

Abstract: Nowadays, performing dynamic line scan thermography (DLST) is very challenging, and therefore an expert is needed in order to predict the optimal set-up parameters. The parameters are mostly dependent on the material properties of the object to be inspected, but there are also correlations between the parameters themselves. The interrelationship is not always evident even for someone skilled in the art. Therefore, optimisation using response surface can give more insights in the interconnections between parameters, but also between the material properties and the variables. Performing inspections using an optimised parameter set will result in high contrast thermograms showing the size and shape of the defect accurately. Using response surfaces to predict the optimal parameter set enables to perform fast measurements without the need of extensive testing to find adequate measurement parameters. Differing from the optimal parameters will result in contrast loss or detail loss of the size and shape of the detected defect.

Keywords: dynamic line scan; active thermography; response surfaces; optimisation

1. Introduction

Active thermography is recognised worldwide as a promising technique to perform non-destructive inspections [1]. The technology found its place in diverse domains compared to before when the technique was mainly used in the aerospace industry. The main drawback of performing active thermography measurements on large samples was the fact the thermal camera or the structure had to moved in order to inspect the whole object. Moving the camera or object in multiple steps is highly sensitive to mistakes and therefore a solution was developed by NASA. The technique was based on the ideas of Maldague [2] and Lindberg [3] of moving the camera and heat source in tandem. When combining the heat source and the camera in a solid set-up, the heating direction, homogeneity, distance, etc. are the same for every frame. Constraining the heat source and the camera together enables optimisation of the measurement set-up in an accurate way. In Figure 1, a visualisation of a Dynamic Line Scan Thermography set-up with the most important parameters is shown.

Several studies have been performed in order to optimise a Dynamic Line Scan Thermography set-up. Most of this optimisation research focuses on a specific use case or a specific material group [4–6]. Dynamic Line Scan Thermography (DLST) is often linked with carbon fibre-reinforced plastic parts used in the aerospace industry. The technique, however, is also used for different cases such as paper, wood, concrete, etc. [7]. Optimising the measurement setup in order to inspect a certain sample results in showing that it is possible to use DLST. Peeters et al. [6] used finite element updating in order to find the best parameter set for the sample to be inspected. The aim of this research is to provide a general

optimisation routine based on response surfaces. Instead of performing an optimisation for a specific use case, the correlation between the set-up variables and the measured contrast is investigated. Response surfaces are widely used in order to find an optimum while reducing the amount of computationally intensive simulations [8–10]. Performing optimisations using response surfaces is used in a variety of applications [11–14], and the use of response surfaces is still being optimised [15]. As can be seen in Figure 1, there are many parameters that influence the optimal measurement set-up for DLST. Some of these parameters can be hard to assess such as the defect diameter and the starting depth of the defect. During production, a person involved in the process can estimate the common properties of defects inside the object. The measurement set-up could be optimised for these estimated properties using a computationally expensive optimisation. If the estimations were faulty, an additional optimisation should be performed, resulting in supplementary simulations. Each variation in a parameter results in the necessity to perform a new optimisation, and therefore the use of response surfaces is justifiable. This paper discusses the creation of the response surface used for the optimisation and offers an explanation for the influence of every variable used. How the response surface is employed in this research is described in the second part of this paper. Performing thermal inspections based on the optimised parameters is explained in part three.
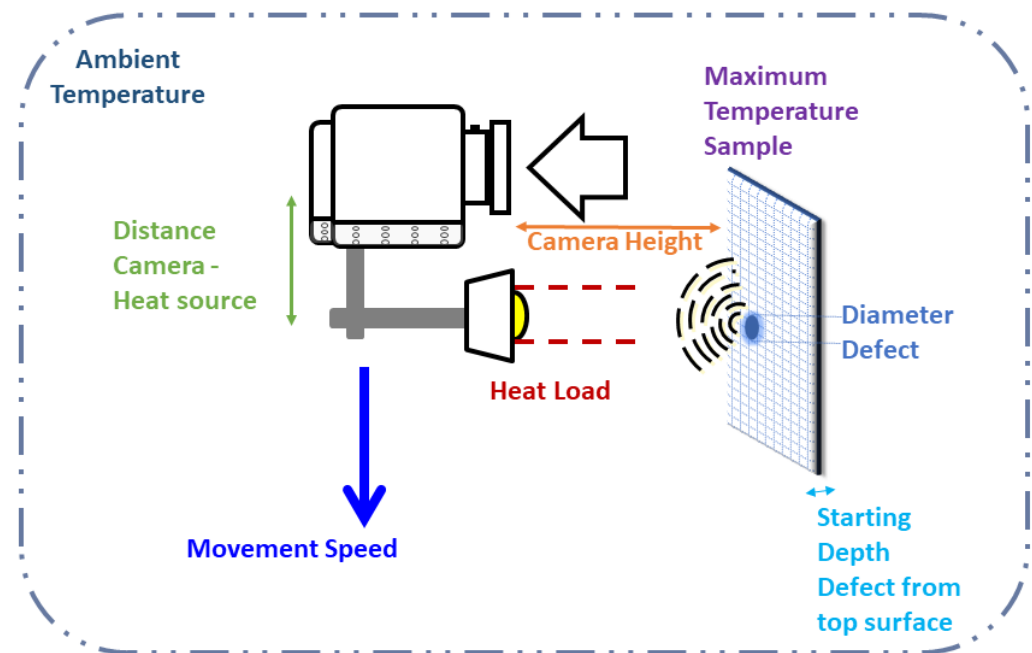

Figure 1. Visualisation of a Dynamic Line Scan Thermography set-up with the most important parameters to be optimised. The parameters in the representation are the input parameters of the response surface, except the maximum temperature is a constraint.

2. Materials and Methods

2.1. Finite Element Simulation

A finite element simulation was created using Siemens Simcenter 3D. The simulation consists of a flat bottom hole plate with one circular cavity and a moving heat source above it. A visualisation of the geometry of the simulation can be found in Figure 2 and the complete simulation in Figure 3.
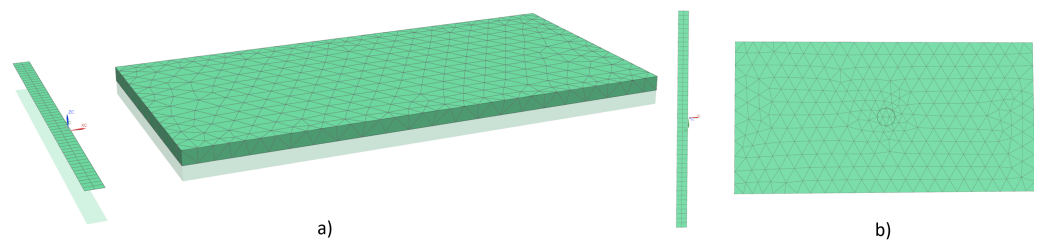
Figure 2. Visualisation of the finite element simulation. (**a**) A 3D representation from the top in order to clearly see the flat bottom hole plate and the 2D mesh for the moving heat source. (**b**) Bottom view of the components. The circular void is placed in the middle of the flat bottom hole plate.

2.1.1. Flat Bottom Hole Plate

The flat bottom hole plate is a rectangular cuboid with following dimensions: $330 \times 170 \times 10$ mm. The dimensions are chosen in order to minimise the influence of the sides during the simulations. Edges cool down differently than the area in the middle of a sample. As the optimisation routine focuses on dynamic measurements, a longer sample is desirable. The thickness of 10 mm is chosen as it is most of the time considered as the maximum depth at which defects can be distinguished using active thermography. The dimensions of the flat bottom plate can be chosen freely as they do not influence the effect of each parameter on each other and on the contrast. Therefore, the dimensions are chosen to match the dimensions of the flat bottom hole plate that are used for the experimental measurements. The circular cavity is located in the middle of the plate at the bottom. The dimensions of the cavity are not fixed as these will be varied in order to create a response surface depending on the diameter and the depth of the cavity. A tetrahedral mesh is used on the flat bottom hole plate with a mesh size of 16.4 mm. The material linked to the 3D mesh is PVC since this is a widely used material for testing new thermography methods. A radiation and a convection constraints are placed on the top and sides of the flat bottom hole plate since the sample lays on the bottom side. The used constraints can be found in Table 1. The ambient temperature is used as initial condition on the whole flat bottom hole plate.

Table 1. Settings used in finite element simulation.

Radiation	Simple radiation to environment: GBVF 1 (Gray Body View Factor)
Convection	Convection to environment: Inclined Plate, Top, Multiplier 1
Thermal Diffusivity PVC	0.08 mm^2/s

2.1.2. Moving Heat Source

The heat source is simulated as a 2D mesh with a "radiative heating Simulation Object" in order to mimic the heating region of a line heater. The size of the heated region is derived from the heating region of a commercially available line heater: Mehler Engineering Services [16]. The heated region has a width of 10 mm at a height of 15 mm above the sample to be inspected, as measured in [17].

There exist multiple approaches to simulate Dynamic Line Scan Thermography inspections. One method relies on the movement of the sample underneath the heat source. The opposite approach is to move the heat source and thermal camera over the sample to be inspected. This second method is used in the research as it is less computing intensive.The 2D mesh representing the heating region has less mesh elements than the meshed flat bottom hole plate. The movement is accomplished by using a "Solid Motion Simulation Object" on the 2D mesh in the longitudinal direction of the flat bottom hole plate.
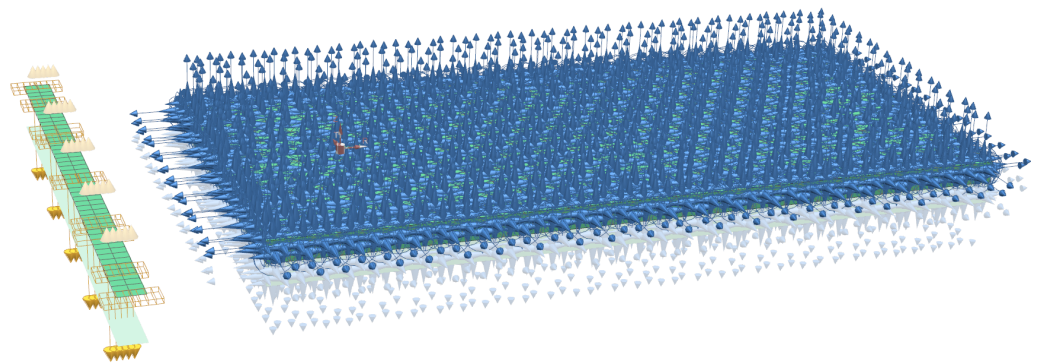
Figure 3. Simulation file representation including constraints and simulation objects. The radiation and convection constraints are only placed on the top and side faces of the flat bottom hole plate as the sample lays flat on the bottom surface. The ambient temperature is applied on every surface as an initial condition.

2.2. Response Surface Parameters

In order to generate a general response surface for DLST measurements, the most important parameters are used as input parameters. The input parameters can be divided in parameters declaring the size of the defect in the flat bottom hole plate and parameters describing the measurement setup. The output parameter visualised in the response surface is the temperature difference between the temperature measured on the surface of the flat bottom hole plate above the middle of the defect and a reference temperature next to the defect. The sound area is chosen next to the defect in order to be heated at the same time as the defect. The exact location is chosen at one centimetre from the edge of the sample. Placing the reference too close to the edge of the sample will result in biased information as the side of a sample cools down differently than the region in the middle of the sample. As the diameter of the defects is limited in the creation of the response surface, a minimal distance between the sound area and defective area is always minimal 50 mm. The temperature difference is used as the output parameter as thermographic inspections rely on the temperature contrast between defect and sound regions. Despite the temperature difference being the most important output parameter a response surface is also created from the temperature above the defect. This response surface will serve as a way to prevent the sample from reaching its maximum use temperature.

2.2.1. Defect Diameter—D_{defect}

The size of a defect has a direct influence on the amount of energy being reflected towards the surface of the flat bottom hole plate. A bigger defect reflects more energy and vice versa. Figure 4 shows the heat transmission through material. The energy injected in the sample travels via conduction through the material. Therefore, the energy can be seen as a thermal wave expanding in all directions. The diameter for this research varies between 6 and 50 mm.

2.2.2. Defect Starting Depth—d_{start}

A deeper laying defect will be less visible using active thermography than a sub-surface defect. As can be seen in Figure, the focused heating disperses as soon as it hits the surface of the flat bottom hole plate. The farther the heat wave has to travel before reflecting on a defect, the smaller its energy density will be. Therefore, the energy density of the heat wave reflected on the defect is strongly dependent on defect depth. Deeper-laying defects will result in less contrast at the surface when inspected. As the sample has a thickness of 10 the start depth limited to 9 mm and the minimum startdepth is 0.1 mm.
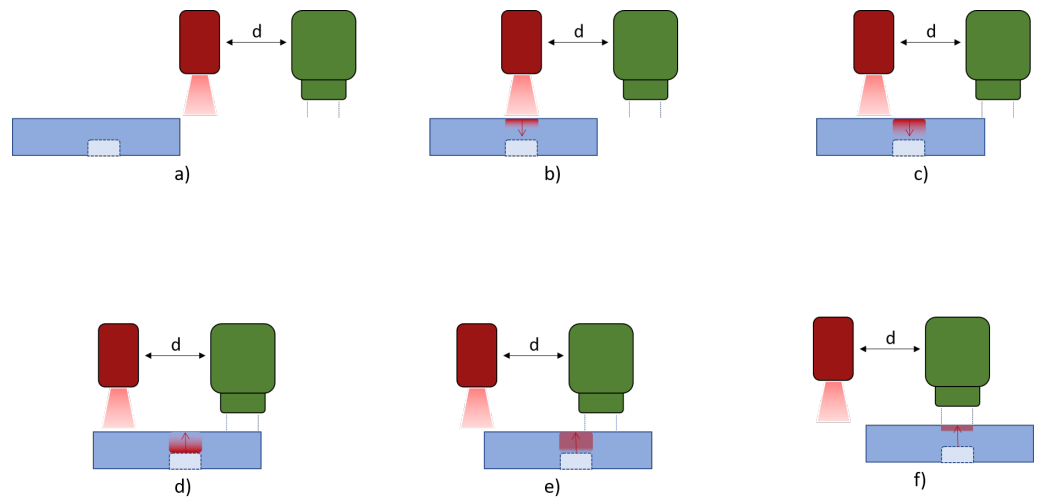
Figure 4. The distance between the heat source and the thermal camera has utter importance in maximising the temperature difference between a sound region and a defect region. The heat wave injected in the sample to be inspected needs an amount of time to reach the defect and to reflect towards the surface. This period is dependent on the depth of the defect and the material properties. A visualisation of the travelling heat wave in an optimised scenario can be seen in multiple steps starting at subfigure (**a**–**f**).

2.2.3. Heat Load—P_{heat}

The heat load has a direct influence on the contrast in thermograms caused by a defect in the object to be inspected. As the induced heat has to travel through the sample towards the defect, be reflected and travel back to the surface, more induced heat will result in more reflected energy. The value of the heat load lay between 100 and 1000 W.

2.2.4. Source Velocity—v_{source}

The movement speed of the heating source has a dual influence on the contrast caused by the defect. On the one hand, the source velocity has a connection to the available time for a specific region of the sample to be heated, and on the other hand, the movement pace is linked to the optimal moment to inspect the object with the infrared camera. The heat wave originating from the induced energy needs a certain amount of time to reach the defect and reflect towards the top surface of the object to be inspected. The needed period is solely dependent on the depth of the of the defect and the material properties of the sample. Using an inadequate tempo will result in measuring the temperature while the heat wave has not yet reached the surface or while the heat wave has reached the surface a decent time before. The source velocity is demarcated between 5 and 20 mm/s.

2.2.5. Distance between Heat Source and Thermal Camera—$d_{heat-cam}$

The second mentioned influence of the source velocity can be minimised by implementing an additional parameter: the distance between heat source and thermal camera. The optimal distance between the heat source and the thermal camera is dependent on the movement speed of the heat source relative to the sample to be inspected and the starting depth of the defect measured from the top surface. A visual representation can be found in Figure 4. The optimal spacing between the heat source and the camera is the distance where the time needed for a sample section to travel from the heat source towards the camera equals the required time for the heat wave to travel through the sample, reflect on the defect and return to the surface. Equation (1) represents this constraint. The minimal distance is 50 mm and the maximum distance is 600 mm for this research.

In an optimised occasion, the time needed for the heat wave to propagate through the sample twice is equal to the time calculated by

$$t_h = \frac{d_{heat-cam}}{v_{source}} \tag{1}$$

where t_h represents the time needed for the heat wave to reach the defect and reflect to the surface, $d_{heat-cam}$ the distance between the heat source and the camera and v_{source} the velocity of the heat source relative to the sample.

2.2.6. Height Thermal Camera—d_{height}

The distance measured from the sensor of the thermal camera to the surface of the sample to be inspected is represented by the height of the thermal camera. This parameter has no influence on the temperature difference of the sample surface, but it is utterly important while performing thermal inspections. In order to measure a defect accurately, the size of the hotspot has to be at least 3 pixels in diameter. This rule of thumb results in a correlation between the height of the thermal camera and the minimal size of the detectable defect. This parameter can be calculated using the Field Of View of the camera as well as using the focal length of the lens. In this research the focal length is used; the calculation using the Field Of View (FOV) can be found in [6].

As can be seen in Figure 5, we can use opposite angles in order to describe the correlation between the pixel pitch p and the minimal size of a defect at a certain camera height d.

$$h = d * \frac{\frac{p}{2}}{f} \tag{2}$$

with h size of the inspected region by half a pixel, p the pixel pitch and f the focal length of the lens. As we are interested in the dimensions of a region captured by one whole pixel the calculated size h has to be doubled.
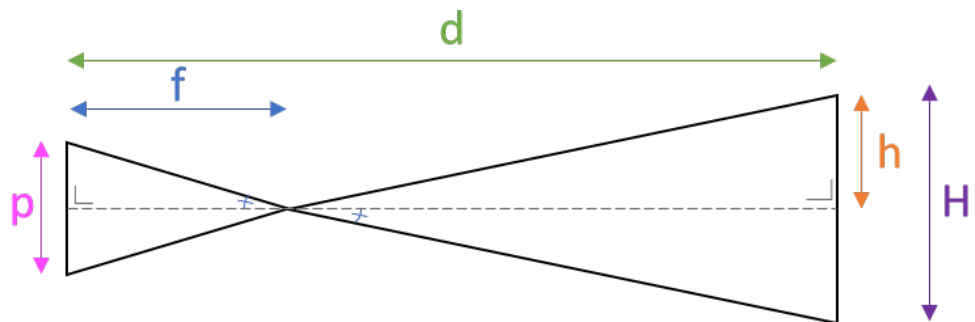
$$H = 2 * h \tag{3}$$

Figure 5. Schematic representation used to calculate the minimum defect diameter in order to be detectable for a certain camera height d. Using the detector pitch of the camera and the focal length of the lens the region recorded by one single pixel H can be calculated.

In order to determine the minimal dimensions of a defect to be detectable at a certain camera height one should know how many pixels are needed in order to perform a decent thermography measurement. A rule of thumb indicates that a defect has to be bigger than a square of 3×3 pixels, therefore the diameter of a round hole has to be at least 3 times the region measured by a single pixel.

$$D \geq 3 * H \tag{4}$$

Combining Equations ([2](#)) and ([4](#)) results in following equation:

$$D \geq 6 * d * \frac{\frac{p}{2}}{f} \tag{5}$$

with D being the minimal diameter of a defect in order to be detectable for the camera at height d_{height} above the sample to be inspected.

2.2.7. Ambient Temperature—$T_{ambient}$

The ambient temperature has an influence on the measured temperatures during the thermography inspections. There is no direct correlation with the measured temperature difference, but it is utterly important to the maximum use temperature. The higher the ambient temperature, the less power has to be added in order to reach this temperature.

2.2.8. Case-Specific Parameters

The parameters discussed above are only dependent on the material properties of the sample to be inspected. As can be seen in [6], the image acquisition rate, frame rate of the camera and the scanning path of the inspection are not considered in this research. The frame rate of the camera has no influence on the response surface as the optimal measurement moment is calculated using the distance between the heat source and the camera. The time difference between passing the heat source and the camera is calculated. Therefore, the amount of frames can change accordingly to the frame rate, but the time remains the same. The scanning path is not taken into account as path optimisation is tremendously dependent on the use case. Inspections whereby the width of the sample is smaller than the heat source have no need for additional path optimisation. Two-dimensional inspections can be partly optimised using the parameter optimisation of this research. There will remain the possibility for further path optimisation, for example, by implementing the pre-heating of a sample region, etc. As these parameters are so specific, they will not be taken into account for this research.

2.2.9. Constraints

One could think that the contrast can be maximised by using the maximum heat load and the minimum source velocity. This actually could work, however one could not call this optimising the use of dynamic line scan thermography. In order to optimise the set-up parameters, constraints have to be imported depending on the case. An utterly important constraint is the maximum temperature of the sample to be inspected as this can not reach the maximum use temperature. This constraint always remains in force, but one can imagine temporary constraints depending on the case. In mass-production environments, the velocity of the sample on the conveyor belt could become a constraint as well. In this case the optimisation problem shifts from finding the highest temperature difference to finding the biggest contrast considering the minimal speed or a fixed speed. It is also possible to change the way of thinking and optimise the parameters in order to use as little power as possible. In order to have the freedom to add or remove constraints response surfaces were used in stead of an optimisation for each scenario.

2.3. Response Surfaces

In order to preserve the freedom of adding and or removing constraints without the need of running an optimisation simulation, response surfaces are used in this research. The response surfaces were created using specialised software to perform multiple simulations, named Siemens Heeds. This software is used for design space exploration and therefore combines multiple software packages such as Siemens Simcenter 3D, Python, etc. Multiple simulations are performed using a variety of parameter sets. The output for every simulation is plotted and stored together with the parameter set and a surrogate surface is learned from this data. This surrogate will be used in order to predict the optimal parameter set based on the constraints. In order to create an accurate surrogate, 1000 simulations

were performed in the complete design space. The design exploration software used in this research has the ability to draft the response surface in several ways such as Least squares linear, Least squares quadratic, Kriging gaussian, Radial Basis Function (RBF) thin plate spline and one can even program a new approximation himself. In this research, RBF thin plate spline approximation is used.

2.3.1. Correlation Table

Using the design exploration software a correlation table is created using the multiple simulations. Using the correlation table one can see interesting and unexpected correlation between several parameters. One can see a correlation table extracted from the simulations in Figure 6.
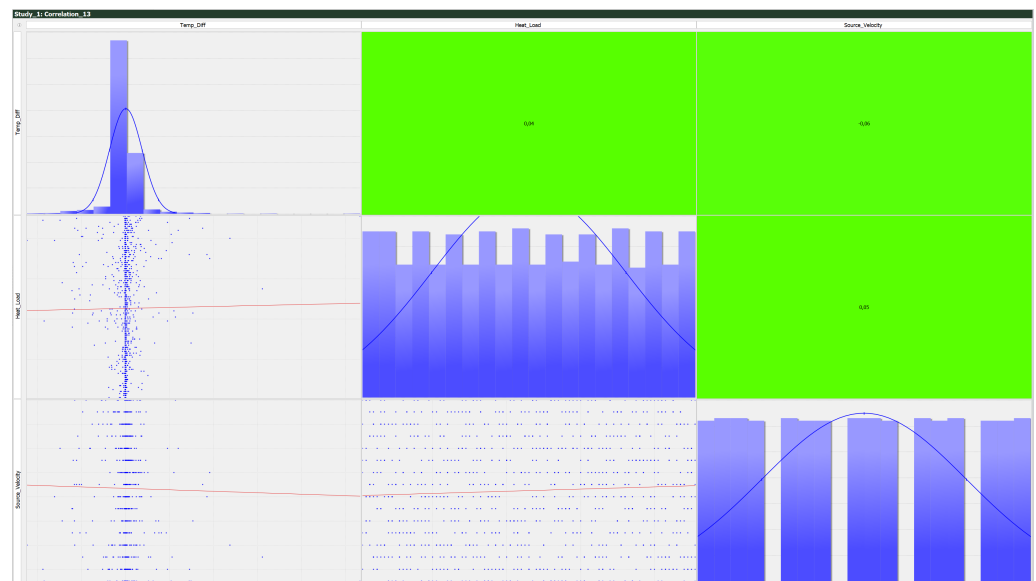

Figure 6. A correlation table drawn up while performing the 1000 simulations needed to create the response surface. The chosen parameters are placed on the x- and y-axis in order to get a relation between the parameters separately. The connections represented in the table are solely linearly approached, resulting in non-accurate approximations. The colour of each box gives a visual representation of the correlation between the parameters. One should inspect the dispersion of the measurement points for one parameter in order to find the correlation as the linearly approximation is faulty. This visualisation focuses on the influence of the heating power in combination with the source velocity in order to predict the resulting temperature difference. A correlation table can be drawn for every parameter combination as wanted.

2.3.2. Simplified Surfaces

It is only possible to make visual representations of 3D response surfaces; therefore, only two input parameters can be evaluated regarding the resulting contrast. As the total response surface has more input parameters than two it is not feasible to create a visual representation of the response surface. Creating the visualisations can help to understand the correlation between several input parameters. This knowledge can be useful in order to optimise a set-up where multiple parameters are fixed as a result of an already existing inspection set-up. In Figure 7, one can see a 3D visualisation showing the influence of the heat load and the source velocity on the temperature difference for a set of fixed parameters.
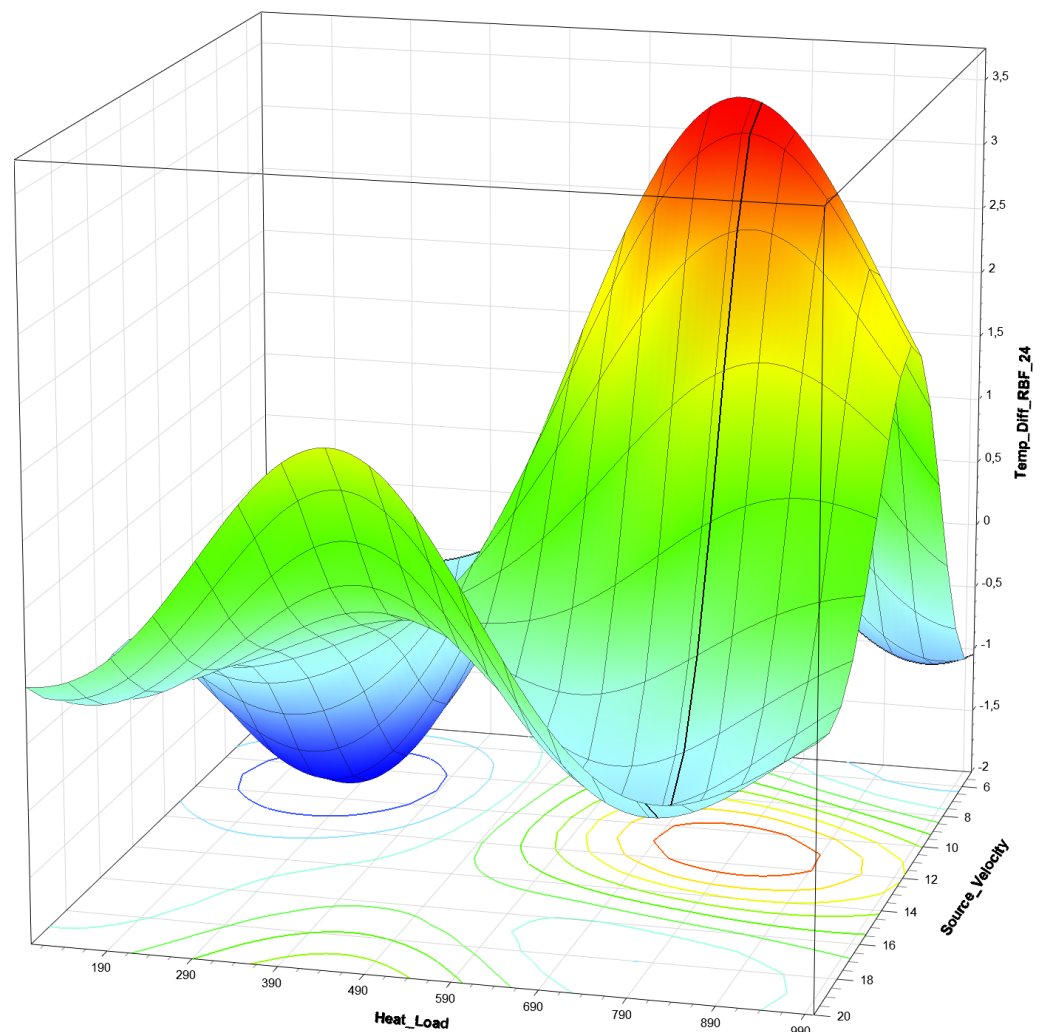
Figure 7. A simplified 3D response surface extracted from the eight dimensional response surface created using 1000 DLST simulations. An approximation has been composed visualising the influence of the source velocity [mm/s] and the heat load [W] on the contrast above the defect [°C]. The following values are used for the remaining parameters: $d_{heat-cam}$ = 425 mm, d_{start} = 5.8 mm, D_{hole} = 9 mm, d_{height} = 430 mm, $T_{ambient}$ = 48 °C. An ambient temperature of 48 °C is extremely high, but as it does not influence the temperature difference, this example is chosen to show that the response surface can be created under extreme circumstances as well. One can clearly see the peak and valley in the response surface and therefore one can find a combination that results in a high contrast. It is important to notice that a 3D visualisation of a response surface only counts for the specific parameter set. One can see that the optimal case is not found for the combination of a maximum heat load and a minimal source velocity. The answer to this phenomenon can be found in the use of the temperature difference as output parameter of the response surface. Combining maximum power with minimum velocity will result in the highest surface temperature of the sample, but will not automatically result in the biggest temperature difference as the sound area is heated extremely as well.

2.3.3. Joint Response Surface

As can be read in Section 2.3.2, it is only possible to visualise a 3D response surface for a specific parameter set of the remaining parameters. Performing the simulations a joint response surface is created for all parameters simultaneously. This approximation is exported as a Python script that describes the response surface using several parameters. A software tool is programmed in Python in order to predict the best parameter set according to the constraints provided by the inspector. The purpose of this optimisation is to maximise

the temperature difference while taking the fixed parameters in account. The user has to enter some parameters in order for the script to function. The obligated parameter values are the estimated start depth of the defect, the estimated diameter of the the defect, the maximum use temperature of the sample to be inspected and the ambient temperature while performing the inspections. One can consider the estimated defect parameters as the minimal defect size and depth one wants to be able to detect. The distance between the heat source and the camera, the height of the camera, the source velocity and the heating power can be provided if they need to be fixed. Performing the inspections in line with the manufacturing process has a consequence for the parameters that can be optimised. It is not desirable to change the speed of the manufacturing process, therefore every parameter can be given as fixed. The remaining parameters will be optimised considering the given parameters.

3. Results

The measurements were performed on a PVC flat bottom hole plate with a thickness of 9.8 mm and a hole pattern consisting of 12 holes with various depth and diameter. The diameters increase step by step between 6 and 25 mm: 6 mm, 12 mm, 20 mm and 25 mm. The hole depths vary between 2.5 and 8.5 mm: 2.5 mm, 5.5 mm and 8.5 mm. A visual representation can be found in Figure 8. As the used measurement technique is dynamic line scan thermography, the pulse length is solely dependent on the movement velocity. The heating is initiated at the beginning of the measurement and remains until the end of the movement. While the sample moves underneath the heater, the pulse length for a specified region can be calculated using the movement speed of the sample.
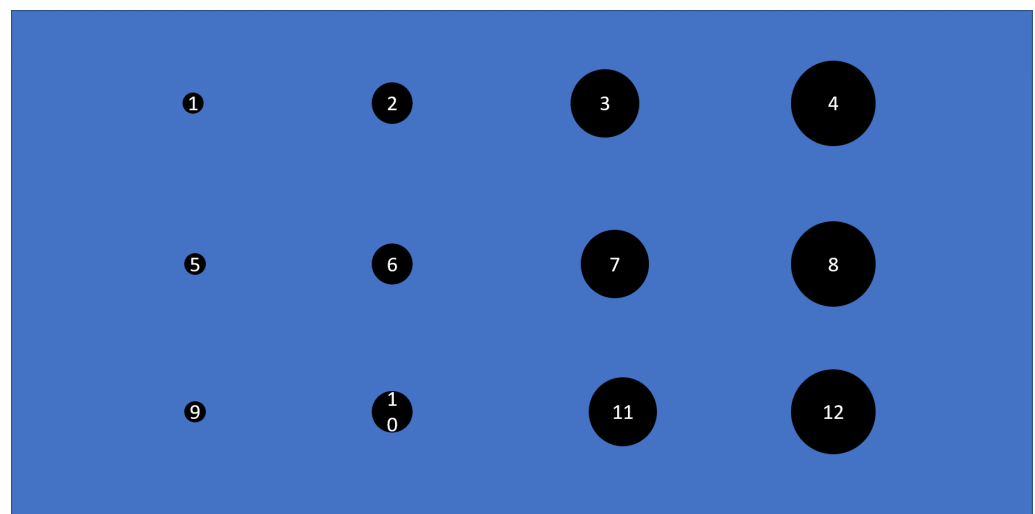

Figure 8. Visual representation of the PVC flat bottom hole plate with various depths and diameters. Holes 1–4 have a depth of 2.5 mm, 5–8 have a depth of 5.5 mm and 9–12 a depth of 8.5 mm. Every vertical set of holes have a different diameter starting with 6 mm for holes 1, 5 and 9. The distance between the centre of the holes is 45 mm in order to minimise the influence of one defect on another.

The parameter set is optimised for hole 2 and resulted in following combination: $d_{heat-cam}$ = 50 mm, P_{heat} = 16.7 W/cm^2, v_{source} = 5 mm/s, d_{height} = 300 mm, $T_{ambient}$ = 22 °C, d_{start} = 2.5 mm, D_{hole} = 12 mm and Maximum use temperature of 80 °C. Optimising the parameter set for hole 2 will result in the upper horizontal row to be detectable in the inspections. The diameter difference has minimal influence on the optimised parameter set. The diameter however will determine the maximal height placement of the camera.

One could see the influence of varying the measurement set-up parameters in comparison to the optimal parameters as predicted by the response surface in Figure 9. Performing measurements at higher speeds without varying the rest of the parameters will result in a loss of contrasts. Placing the camera at a bigger distance from the heat source than

prescribed by the optimised parameter set will result in a minor contrast loss but will majorly result in a loss of detail about the size and shape of the detected defect.
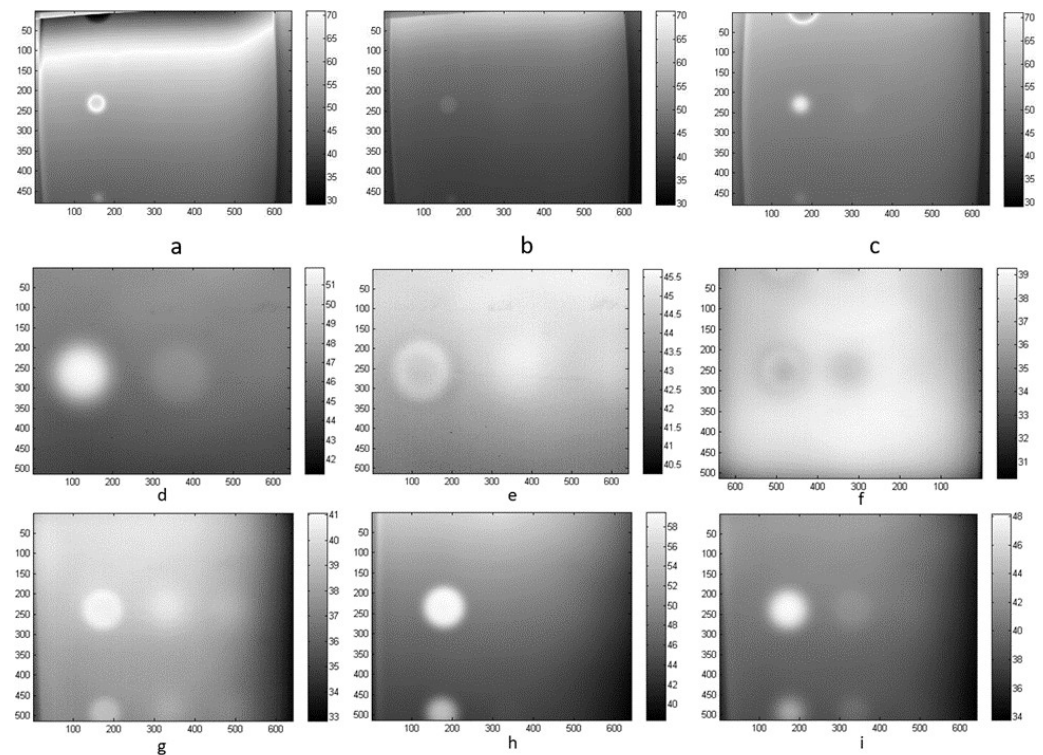

Figure 9. Comparison between measurements performed with alternating parameter set. The values on the *x*- and *y*-axis are pixel values and the colours represent temperatures in °C. The range is fixed between 29 and 70 °C for measurements (**a–c**) in order to facilitate the comparison between different measurements. Image a shows the detection of hole 2 using the optimal parameter set ($d_{heat-cam}$ = 50 mm, P_{heat} = 41.7 W/cm^2, v_{source} = 5 mm/s, d_{height} = 300 mm, $T_{ambient}$ = 22 °C, image b shows the detection of hole 2 with the only difference that the inspection was performed with higher source velocity (15 mm/s) and image c shows the detection of hole 2 using a bigger distance between the camera and heat source (170 mm). As this is a snapshot taken from the DLST measurement other defects are not clearly visible in these images. The defects 1–4 were all clearly visible in the movie what can be explained by the fact that they have the same depth. Other holes such as 7 and 8 could be detected in the movie as well, but were not as clear as hole 2. Measurement (**d–f**) are performed on hole 8, whereby d is measured using the optimal parameter set, e is performed with a movement velocity of 15 mm/s and in measurement (**f**) the camera was placed too close to the heat source (150 mm in stead of 350 mm). The bottom row of measurements (**g–i**) are measurements performed on hole 12. Image (**g**) represents the optimal measurement where hole 12 can barely be detected. In measurement h, the movement speed was 15 mm/s while the optimal speed is 5 mm/s. The difference between g and i is the difference between the heat source and the camera. The distance equals 300 mm for measurement (**g**) and 250 mm for measurement (**i**).

The optimal parameter set for each hole can be found in Figure 10.

In order to compare the contrast objectively the contrast is calculated between a pixel in the centre of defect on eight different pixels around the defect. The location of the pixels is shown in Figure 11. The contrast is calculated as the absolute value of the sum of the temperature difference between a pixel and the centre pixel divided by 8.

Hole	Diameter [mm]	Depth [mm]	Distance Heat source - camera [mm]	Heating Power [W]	Source velocity [mm/s]	Camera Height [mm]	Ambient Temperature °C	Maximum use temperature°C	Contrast °C
1	6	2.5	50	300	7	300	22	80	16
2	12	2.5	550	900	19	950	22	80	8.9
3	20	2.5	150	400	19	300	22	80	12.1
4	25	2.5	50	600	19	300	22	80	27.7
5	6	5.5	50	300	5	300	22	80	34.2
6	12	5.5	50	900	5	300	22	80	15.8
7	20	5.5	100	800	10	950	22	80	10.4
8	25	5.5	350	300	5	950	22	80	27.3
9	6	8.5	50	800	17	300	22	80	12.5
10	12	8.5	50	500	5	300	22	80	7.7
11	20	8.5	250	900	16	950	22	80	13.4
12	25	8.5	300	300	5	950	22	80	29.2

Figure 10. Optimal parameter sets found for the holes in the flat bottom hole sample. The ambient room temperature is 22 °C and the maximum use temperature is chosen at 80 °C. This is not the maximum use temperature of PVC, but it limits the cooling time the sample needs before performing a consecutive measurement. As the temperature difference is used as a measure of contrast, this limitation of the maximum temperature causes no problems. Next to the optimal parameter values for each parameter, the predicted temperature difference is calculated. This contrast is calculated between the sound area and the area above the defect.
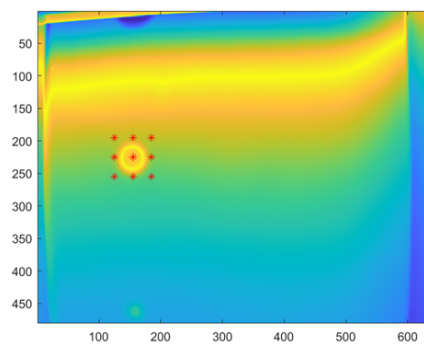
a	0,3590
b	0,0156
c	0,1638

Figure 11. Calculation of the contrast between 9 pixels. The centre pixel is situated in the middle of the defect and the other defects are spaced equally around the centre pixel. The distance between the pixels is 30 pixels. The contrast values are calculated for the images (a–c) of Figure 9. A higher value equals a bigger contrast between the defect and the surroundings.

4. Discussion

The optimisation routine presented in this research can offer an insight in the working principle of dynamic line scan thermography. Understanding the influence of the different parameters on each other helps an inspector select the most appropriate measurement set-up, reducing the time needed to perform inspections. In addition, it enables us to perform measurements without the need of an expert skilled in the art of thermography. It should be mentioned that the presented technique assumes that the defects are sufficiently distant from each other. Defects near one another will influence the contrast shown in the thermograms. The influence is shown in Figure 12. As can be seen bigger defects experience less influence of nearby defects as the reflected energy is greater. Defects starting at different distances beneath the top surface however will minimally influence each other.
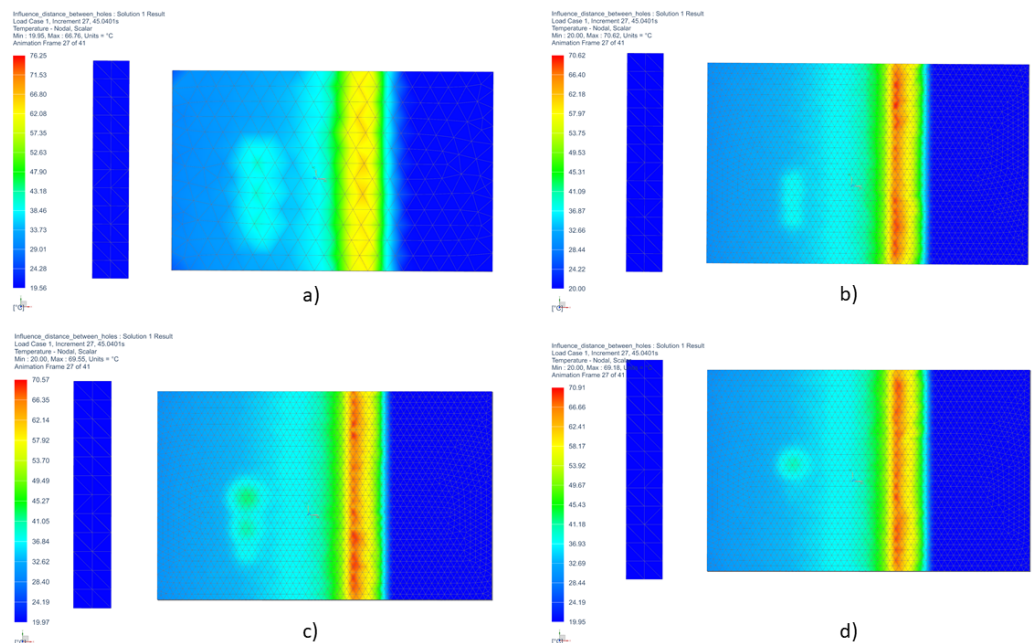
Figure 12. The influence of the intermediate distance between samples on the contrast is visualised in four situations. Image (**a**) represents a simulation of three defects with a diameter of 25 mm, a depth of 5 mm under the surface and an intermediate distance of 27 mm between the centres of the defects. The heat reflected by the defects influences each other resulting in a reduction of the contrast between the separate defects. The resulting hotspot is bigger than the area of the defects. Visualisation (**b**) represents a similar simulation performed on defects of 12 mm diameter, starting 5 mm underneath the top surface and at an intermediate distance of 15 mm of each other. The heat reflected by the separate defects influences the contrast making it impossible to distinguish the defects. Smaller defects, however, reflect less energy in comparison to bigger defects making it harder to detect them. Multiple small defects close to each other will show as a bigger defect, but with more contrast than the individual defects. Defects of different diameters are simulated in subfigure (**c**) where the intermediate distance is 25 mm between the defects. The defects have diameters of 25 mm, 20 mm and 12 mm. The two bigger defects can still be distinguished from each other. The smallest defect however shows as a part of the other defect. Subfigure (**d**) shows the influence of defects placed at different starting depths from the top surface. The defects all have a diameter of 25 mm and are placed at a depth of 5 mm, 10 mm and 15 mm underneath the surface. As the heat wave requires a specified amount to reach the top of the defect and reflect to the top surface, the different defects will not result in hotspots at the same moment in the inspection. Therefore, the influence of deeper defects will effect the top defect minimally. Deeper defects, however, will be less visible to detect because of the hotter regions caused by defects above. The defects closest to the surface will not have the biggest contrast since the parameters are not optimal, but they will still remain hot, disturbing the detection of defects at a greater distance from the top surface. This occurrence makes a flat bottom hole plate with defects at different depths not the most suitable test case.

5. Conclusions

Performing dynamic line scan thermography measurements is a difficult task without consulting an expert. The various parameters have an impact on each other, making it challenging to estimate the correlation between one and another. Using a response surface however, it is possible to find the best parameter set based on the defect parameters such as diameter and depth beneath the inspected surface. The algorithm to find the optimal parameter set focuses on maximising the temperature difference between the area above the defect and a sound area. In order to prevent the sample from overheating a maximum use temperature can be given as input parameter next to the defect parameters and the ambient temperature. The resulting parameter set consists of following parameters: Defect

Diameter D_{defect}, Defect Starting Depth d_{start}, Ambient Temperature $T_{ambient}$, Maximum Use Temperature, Heat Load P_{heat}, Source Velocity v_{source}, Distance Between Heat Source and Thermal Camera $d_{heat-cam}$ and Height Thermal Camera d_{height}. Measurements performed with an optimised parameter set result in good contrast rapidly. Differing from the optimised parameter set will result in contrast loss and even losing the possibility to detect the defects. This research paper only focused on the creation of a response surface for DLST measurements on PVC samples as this is the standard testing material for thermography. In order to increase the usability of the technique in the industry, the routine will be expanded towards a general optimisation. The material properties of PVC will be replaced by additional input parameters for the response surface. Therefore, it should become possible to predict the optimal parameter set for each material. A solution will be searched to calculate the influence of nearby defects in the prediction of the optimal parameter set.

Author Contributions: S.V.: Conceptualization, methodology, writing—original draft preparation and data curation; J.G.: software; B.R.: Conceptualization and writing—review and editing; X.M.: writing—review and editing and supervision; G.S.: writing—review and editing, supervision and resources. All authors have read and agreed to the published version of the manuscript.

Conflicts of Interest: The authors declare no conflict of interest.

References

1. Xavier P. Maldague. *Theory and Practice of Infrared Thermography for Nondestructive Testing*; Wiley: New York, NY, USA, 2001.
2. Maldague, X. *Nondestructive Evaluation of Materials by Infrared Thermography—Xavier P.V. Maldague—Google Boeken*; Springer: Berlin, Germany, 2012.
3. Lindberg, P.J. A Prism Line-scanner for High-speed Thermography. *Opt. Acta Int. J. Opt.* **1968**, *15*, 305–316. [CrossRef]
4. Ibarra-Castanedo, C.; Servais, P.; Ziadi, A.; Klein, M.; Maldague, X. RITA—Robotized Inspection by Thermography and Advanced processing for the inspection of aeronautical components. In Proceedings of the 12th International Conference on Quantitative InfraRed Thermography, Bordeaux, France, 7–11 July 2014; [CrossRef]
5. Ley, O.; Godinez-Azcuaga, V. *Line Scanning Thermography and its Application Inspecting Aerospace Composites*; Technical Report; Mistras Group, Inc.: Princeton Junction, NJ, USA, 2013.
6. Peeters, J.; Ibarra-Castanedo, C.; Khodayar, F.; Mokhtari, Y.; Sfarra, S.; Zhang, H.; Maldague, X.; Dirckx, J.J.; Steenackers, G. Optimised dynamic line scan thermographic detection of CFRP inserts using FE updating and POD analysis. *NDT E Int.* **2018**, *93*, 141–149. [CrossRef]
7. Zhang, H.; Sfarra, S.; Ibarra-Castanedo, C.; Maldague, X.P. Dynamic Line-Scan Thermography for the Inspection of Paper-Based Materials: A Case Study Focused on an Ancient Book Cover. *Proceedings* **2019**, *27*, 9. [CrossRef]
8. Steenackers, G.; Presezniak, F.; Guillaume, P. Development of an adaptive response surface method for optimization of computation-intensive models. *Comput. Ind. Eng.* **2009**, *57*, 847–855. [CrossRef]
9. Genna, S.; Tagliaferri, F.; Papa, I.; Leone, C.; Palumbo, B. Multi-response optimization of CFRP laser milling process based on response surface methodology. *Polym. Eng. Sci.* **2017**, *57*, 595–605. [CrossRef]
10. Myers, R.H.A.C. *Response Surface Methodology : Process and Product Optimization Using Designed Experiments*; Wiley: New York, NY, USA, 2016.
11. Ghanbarian, M.; Ghanbarian, M.; Mahvi, A.H.; Tabatabaie, T. Enhanced fluoride removal over MgFe2O4–chitosan–CaAl nanohybrid: Response surface optimization, kinetic and isotherm study. *Int. J. Biol. Macromol.* **2020**, *148*, 574–590. [CrossRef] [PubMed]
12. Teglia, C.M.; Guiñez, M.; Goicoechea, H.C.; Culzoni, M.J.; Cerutti, S. Enhancement of multianalyte mass spectrometry detection through response surface optimization by least squares and artificial neural network modelling. *J. Chromatogr. A* **2020**, *1611*, 460613. [CrossRef] [PubMed]
13. Davoodi, B.; Eskandari, B. Tool wear mechanisms and multi-response optimization of tool life and volume of material removed in turning of N-155 iron-nickel-base superalloy using RSM. *Meas. J. Int. Meas. Confed.* **2015**, *68*, 286–294. [CrossRef]
14. Liu, Y.; Zhou, J.; Fu, W.; Zhang, B.; Chang, F.; Jiang, P. Study on the effect of cutting parameters on bamboo surface quality using response surface methodology. *Measurement* **2021**, *174*, 109002. [CrossRef]
15. Alrweili, H.; Georgiou, S.; Stylianou, S. A New Class of Second-Order Response Surface Designs. *IEEE Access* **2020**, *8*, 115123–115132. [CrossRef]

16. Areas, C. MES Thermsol® lineIR CP/CF Infrared Line Radiators for Heating Special Edge, Bend and Connection Areas. Available online: https://www.m-e-s.de/wp-content/uploads/2019/07/MES-thermsol%C2%AE-Informationsmappe-englisch-2014.pdf (accessed on 1 December 2020).

17. Verspeek, S.; Ribbens, B.; Maldague, X.; Steenackers, G. Optimisation of a Heat Source for Infrared Thermography Measurements: Comparison to Mehler Engineering + Service-Heater. *Appl. Sci.* **2020**, *10*, 1285. [CrossRef]